Oil & Gas Science and Technology – Rev. IFP Energies nouvelles, Vol. 69 (2014), No. 7, pp. 1171-1189

DOI: 10.2516/ogst/2013146

Assessing the Permeability in Anisotropic and Weakly Permeable Porous Rocks Using Radial Pulse Tests

Richard Giot*, Albert Giraud and Christophe Auvray

Laboratoire Géoressources, ENSG-Université de Lorraine, UMR 7359, 2 rue du Doyen Marcel Roubault, TSA 70605, 54518 Vandœuvre-Lès-Nancy - France

e-mail: richard.giot@univ-lorraine.fr - albert.giraud@univ-lorraine.fr - christophe.auvray@univ-lorraine.fr

* Corresponding author

Résumé — **Estimation de la perméabilité d'une roche anisotrope très faiblement perméable par pulse tests radiaux** — Le pulse test est généralement considéré comme un essai adapté pour la mesure de la perméabilité des roches poreuses très faiblement perméables. Classiquement, l'essai consiste à imposer un saut de pression à la base d'un échantillon cylindrique et à mesurer les variations de pression dans les réservoirs amont et aval. Dans les présents travaux, nous proposons un nouveau dispositif et une nouvelle procédure sur échantillon de type cylindre creux : le saut de pression est imposé dans un trou axial et la pression mesurée dans le trou et à la circonférence de l'échantillon. Cette configuration génère un écoulement à la fois axial et transversal, et non seulement axial comme dans le cas de l'essai classique. Pour les roches isotropes transverses, cela permet la détermination de la perméabilité dans les directions parallèle et perpendiculaire aux plans d'isotropie, à partir d'un seul échantillon, judicieusement orienté. L'essai est couplé hydro-mécaniquement, et en conséquence aucune solution analytique ne peut être considérée. L'essai est alors interprété en ayant recours à des modélisations numériques couplées HM 3D, prenant en compte l'anisotropie des échantillons. Dans les travaux précédents, une loi poro-élastique isotrope transverse, ainsi qu'une méthode inverse couplée aux modélisations numériques pour identifier des paramètres, ont été développées et implantées dans le code aux éléments finis Code_Aster (Edf). La méthode est adaptée pour l'interprétation de l'essai de pulse radial et appliquée à des échantillons cylindriques creux d'argilites de Meuse/Haute-Marne, avec axe soit perpendiculaire soit parallèle aux plans d'isotropie. Alors que pour l'essai de pulse axial classique, la méthode requiert deux échantillons pour déterminer les perméabilités intrinsèques dans les directions parallèle et perpendiculaire aux plans d'isotropie, la méthode appliquée à l'essai de pulse radial permet la détermination des perméabilités intrinsèques dans ces deux directions sur un seul échantillon. Ceci permet de s'affranchir d'effets d'hétérogénéités des échantillons.

Abstract *— **Assessing the Permeability in Anisotropic and Weakly Permeable Porous Rocks Using Radial Pulse Tests** — The pulse test is usually considered to be an efficient method for measuring the permeability of weakly permeable porous rocks. Classically, the test consists of imposing a pressure drop on the base of a cylindrical sample and measuring the pressure variations in the upstream and downstream reservoirs. In the present work, we propose a new apparatus and procedure for hollow*

cylindrical samples in which the pressure drop is imposed in an axial hole and the pressure is measured both in the hole and on the circumference of the sample. Unlike the classical axial pulse test, this configuration results in a flow in both the axial and transversal directions rather than only in the axial direction. For transverse isotropic rocks, this configuration allows the assessment of the permeability in the isotropy planes and normal to the isotropy planes in a single sample when the samples are appropriately oriented. The test is fully hydro-mechanically coupled; therefore, no analytical solution exists. The test is then interpreted through fully coupled numerical modeling in 3D, considering the anisotropy of the samples. In previous works, we developed and implemented a transverse isotropic poroelastic constitutive law in the finite element code Code_Aster (Edf), as well as an inverse method coupled to the numerical modeling for parameter identification. The method is adapted to the radial pulse test and then applied to hollow cylindrical samples of Meuse/Haute-Marne argillite with the axis either parallel or perpendicular to the isotropy planes. Although this method requires 2 samples for the assessment of permeability in the isotropy planes and normal to the isotropy planes in the axial pulse test, the method applied to the radial pulse test allows the assessment of intrinsic permeability in both directions on a single sample, which allows freeing ourselves from a heterogeneity effect.

NOMENCLATURE

$\boldsymbol{\sigma}$	Second-order stress tensor (Pa)
$\boldsymbol{\varepsilon}$	Second-order strain tensor (-)
σ_m	Mean stress (Pa)
$\mathbf{s}$	Deviatoric stress tensor (Pa)
ε_v	Volumetric strain (-)
$\mathbf{e}$	Deviatoric strain tensor (-)
$\boldsymbol{F^m}$	Resultant of mass forces (N)
m_{lq}	Liquid mass supply ($kg.m^{-3}$)
ρ_{lq}	Liquid density ($kg.m^{-3}$)
p_{lq}	Liquid pressure (Pa)
K_o	Drained bulk modulus (Pa)
K_{un}	Undrained bulk modulus (Pa)
b	Biot coefficient in the isotropic case (-)
b_1	Biot coefficient in the isotropy plane (-)
b_3	Biot coefficient in the direction normal to the isotropy plane (-)
M	Biot modulus (Pa)
λ_{lq}	Darcy's conductivity for liquid ($Pa^{-1}.m^2.s^{-1}$)
k_{lq}	Liquid conductivity ($m.s^{-1}$)
k_{int}	Intrinsic permeability in the isotropic case (m^2)
K_1^{int}	Intrinsic permeability in the isotropy plane (m^2)
K_3^{int}	Intrinsic permeability in the direction normal to the isotropy plane (m^2)
μ_{lq}	Liquid dynamic viscosity (Pa.s)
$\boldsymbol{M_{lq}}$	Hydraulic flow of water ($kg.s^{-1}.m^{-2}$)
p_{re}^u	Pressure in the upstream reservoir (Pa)
p_{re}^d	Pressure in the downstream reservoir (Pa)
M_{lq}^u	Mass of liquid contained in the upstream reservoir (kg)
M_{lq}^d	Mass of liquid contained in the downstream reservoir (kg)
ξ^u	Volume of liquid contained in the upstream reservoir (m^3)
ξ^d	Volume of liquid contained in the downstream reservoir (m^3)
C_{re}^u	Stiffness of the upstream reservoir ($Pa.m^{-3}$)
C_{re}^d	Stiffness of the downstream reservoir ($Pa.m^{-3}$)
S_{re}^u	Upstream reservoir storage coefficient ($kg.Pa^{-1}$)
S_{re}^d	Downstream reservoir storage coefficient ($kg.Pa^{-1}$)
γ_{lq}	Volumetric weight of liquid ($kg.m^{-3}$)
D	Liquid diffusivity ($m^2.s^{-1}$)
S_s	Specific storage coefficient ($kg.Pa^{-1}.m^{-3}$)
K_{sq}	Matrix bulk modulus (Pa)
K_{lq}	Liquid bulk modulus (Pa)
f_0	Initial Lagrangian porosity (-)
E_o	Drained Young's modulus (Pa)
E_1	Young's modulus in the isotropy plane (Pa)
E_3	Young's modulus in the direction normal to the isotropy plane (Pa)
v_o	Drained Poisson's ratio (-)
$\mathbb{C}$	Fourth-order elasticity tensor of the porous medium
$\mathbb{C}^s$	Fourth-order elasticity tensor of the matrix
$\mathbf{B}$	Second order tensor of Biot coefficients (-)
M_ϕ	Pore compressibility (Pa)
$\mathbf{K^{int}}$	Second-order tensor of intrinsic permeability (m^2)
$\boldsymbol{\lambda^{lq}}$	Second-order tensor of Darcy's conductivity ($Pa^{-1}.m^2.s^{-1}$)
ϕ, θ, ψ	Euler angles (°)
g	Gravity acceleration ($m.s^{-2}$)

INTRODUCTION

In weakly permeable porous rocks, such as argillite, liquid and gas transfers are governed by permeability. As a consequence, permeability is a key parameter in most of the engineering applications involving these natural geomaterials, for example, nuclear waste or gas storage (for which they can be used as formation for geological sequestration of CO_2). Consequently, permeability is a key issue and has been widely studied for years. For the range of intrinsic permeability values of weakly permeable porous media, that is 10^{-22}-10^{-20} m^2, the classic measurement techniques based on a permanent flow are not adapted. Indeed, for this range of permeability, it is nearly impossible, in practice, to conduct drained tests. As an alternative, one can use transient flow methods, such as the so-called pulse test proposed by Brace *et al.* [1]. The pulse test allows the assessment of both the intrinsic permeability and specific storage, considering samples fully saturated with one fluid. The specific storage is defined as the volume of water, per unit volume of saturated rock, injected into the pores when exposed to a unit increase of pore fluid pressure. During the pulse test, the intrinsic permeability and the specific storage govern the transient evolution and the final equilibrium of pore pressure distribution, respectively. Classically, the pulse test is assumed to be a one-dimensional pore pressure diffusion problem in the axial direction considering simplifying hypotheses, such as constant mean stress, constant strain or uniaxial strain. The matching solutions are then based on the resolution of a hydraulic diffusion-type equation assuming a decoupling between hydraulic and mechanical behaviours. Under the assumption of constant mean stress, Hsieh *et al.* [2] solved the system of equations and proposed an analytical solution for the pulse test. Neuzil *et al.* [3] utilized this solution to offer a graphical method for identifying both the permeability and the specific storage. The analytical solution for the constant mean stress was also applied by Homand *et al.* [4] for the interpretation of pulse tests on argillites, but with an inverse method rather than a graphical method. Sevaldurai *et al.* [5] also considered the classical 1D solutions of the pulse test on saturated samples for the interpretation of pulse tests on Lindsay limestone. The measured pressure curves were compared to calculated curves obtained with the analytical solution, and they assessed permeability on the order of 10^{-23}-10^{-22} m^2.

Even though solutions considering an uncoupling between hydraulic and mechanical behaviours are widespread, Wang [6] and Adachi and Detournay [7] demonstrated that the pulse test is a fully coupled problem with poroelastic strains coupled with the pore pressure field. Walder and Nur [8] showed that neglecting the poromechanical couplings could result in errors in the assessment of permeability. They showed that this simplification leads to a sample size effect that could result in an error on the order of 50% in the estimation of permeability in tight rocks. The coupling between hydraulic and mechanical responses leads to a three-dimensional or two-dimensional axisymmetrical problem, and an accurate solution can only be determined by coupled hydro-mechanical modeling, for example, with a finite element code.

Giot *et al.* [9] also showed the importance of considering poromechanical couplings through 2D axisymmetrical coupled analysis of the pulse test. They developed an inverse method for the interpretation of the pulse test, associating a fully coupled analysis of the pulse test by finite element modeling to an inversion algorithm for the identification of poromechanical parameters. They focused on intrinsic permeability and parameters influencing the specific storage, more precisely, the Biot coefficient, drained Young's modulus and the reservoirs' stiffnesses. The pulse test can then be viewed as a parameter identification problem. The inverse method consists in minimizing, with a gradient-based optimization algorithm, a cost-function that measures the differences between measured and calculated reservoir pressures (the latter being functions of the parameters to be identified). The method was applied on 4 tests on Meuse/Haute-Marne claystone, and a 2D back analysis accounting for couplings gave more accurate results than a single 1D analysis neglecting these couplings. The quality of the fitting given by both analyses is quite similar, but the values of the estimated parameters are different. Concerning the intrinsic permeability, the difference between parameters estimated in 1D and 2D is approximately 5 to 15%, whereas for the specific storage, it can reach 80%. The results of the 4 tests revealed a transverse isotropy of the argillite.

The present work addresses Meuse/Haute-Marne argillites, which are a potential host for radioactive waste disposal. Numerous experimental studies have been conducted on this claystone and have demonstrated its transverse isotropy. Amongst others, Zhang and Rothfuchs [10] showed a gas permeability ratio of 10 and a Young's moduli ratio of 1.5 between directions parallel and normal to the isotropy planes. For partially saturated samples, Cariou *et al.* [11] showed that the anisotropy ratio's effect on argillite stiffnesses increases when water content decreases, whereas the Biot coefficient appears to be isotropic. It is thus essential to consider this anisotropy when conducting permeability measurements on Meuse/Haute-Marne argillites. More generally, when dealing with claystone, Selvadurai *et al.* [5]

underlined the importance of accounting for the anisotropy of rock based on the interpretation of the axial pulse tests they conducted on Lindsay limestone. Marschall *et al.* [12] also reported the intrinsic permeability anisotropy of Opalinus Clay, which was determined through long lasting steady state tests. The order of permeability of this material is 10^{-21}-10^{-20} m^2, with an anisotropy ratio less than 10. Thus, Giot *et al.* [13] adapted their interpretation method of the axial pulse test to account for this anisotropy in the analysis of the test. While studying anisotropy, the 2D fully coupled inversion of the pulse test was replaced by a 3D fully coupled inversion, and a fully coupled transverse isotropic poromechanical model was developed and implemented in the finite element code and then used for the modeling of the pulse test. Nevertheless, they showed that the axial pulse test only allows for the assessment of the permeability in the axial direction of the sample, the flow being only axial. 2 tests on 2 different samples are then required to determine permeability in the isotropy planes and normal to the isotropy planes, which can result in a bias due to heterogeneity effects. Thus, in the present study, we propose a new test, the radial pulse test. This test is performed on hollow cylinders of rock and aims to characterise the whole transverse isotropic permeability, *i.e.*, the intrinsic permeability in the directions parallel and normal to isotropy planes, on one single sample. This method allows freeing ourselves from the heterogeneity of the rock when dealing with different samples and to limit the number of tests. The same approach used for the axial pulse test is used for interpreting the radial pulse test. We make use of the same fully coupled transverse isotropic poromechanical model and inversion procedure to interpret the radial pulse test. Such an inverse problem may have a non-unique solution. Nevertheless, the developed inversion procedure has proven to be efficient in the field of geomechanics, for example, on the axial pulse test (Giot *et al.* [9, 13]) or overcoring (Giot *et al.* [14]), particularly concerning the issues of local minima and the consideration of uncertainties on measurements.

Permeability measurements with hollow cylinders were previously proposed by Alarcon-Ruiz *et al.* [15] on concrete samples of 265 mm height and 350 mm external diameter. The pressure was applied by nitrogen gas rather than with water. The measurements were combined with numerical modeling, without consideration of any mechanical processes, to assess intrinsic permeability. They found permeability on the order of 10^{-16} m^2, which is a rather high permeability and justifies their method for samples of great dimensions. Part of the concrete samples used by Alarcon-Ruiz *et al.* were extracted from a larger sized hollow cylinder that had previously been used for evaluating the intrinsic permeability when submitted to temperature variations. This work was due to Dal Pont *et al.* [16], with the concrete hollow cylinder being 1.5 m high, 0.55 m of external radius with an internal cylinder of 0.25 m. The initial permeability of the concrete is on the order of 10^{-17} m^2, which is also greater than the argillaceous material considered in our case. The gas pressure was measured in the hollow cylinder through 4 cylindrical sensors placed at different distances from the heated surface. This experimental set-up has been coupled to a numerical analysis with a finite element method, and both experimental and numerical results (temperature and gas pressure) have been compared to identify the values of the parameters of the relationship describing the evolution of permeability with temperature.

Even if hollow cylinders have previously been used for relative permeability measurements, none of the previous analyses were aimed at studying the anisotropy of the materials considered, and the sizes of the samples were greater than the one considered in the present study. Moreover, those tests were aimed at identifying gas relative permeability, which is significantly different from water relative permeability in the materials we are concerned with in the present work. Davy *et al.* [17] indicated that water permeability is 2 to 8 orders of magnitude smaller than gas permeability on the same claystone we study in the present work. In terms of physical processes, the radial pulse test is conducted on water-saturated samples and aims to identify intrinsic permeability, which is independent from fluid permeability. There is no gas implied in this test, and thus, there is no need to consider gas diffusion (Fick's law) or even mechanics of partially saturated media. In the present paper, we focus on the pore-pressure diffusion process (in other words, advection, described by Darcy's law) in fully water-saturated medium under isothermal conditions (climate control). Gas diffusion, as described by Fick's law, is not concerned with the present research, or the mechanics of partially saturated media.

1 TRANSVERSE ISOTROPIC COUPLED POROELASTIC CONSTITUTIVE LAW

In this section, we present the main constitutive equations of the transverse isotropic poroelastic model for the saturated case. This model is based on Biot's mechanics for fluid-saturated porous media [6, 27-32]. The corresponding isotropic poroelastic model is available in the finite element code Code_Aster (Edf) [32-33]

and has been detailed in Giot *et al.* [9]. For the Meuse/Haute-Marne (MHM) argillites, we focused on transverse isotropy, with the axis of revolution denoted as O_{x3} and the supposed isotropic behaviour in the plane O_{x1x2}. We assume that the porous medium and the matrix (skeleton) are transverse isotropic elastic with the same symmetry axis O_{x3}.

The full transverse isotropic model is detailed in Giot *et al.* [13]. This model accounts for microscopic parameters and relations between macroscopic and microscopic properties of the constituents. It is an improved version of the model presented in Noiret *et al.* [18]. It is inspired by the anisotropic poroelastic model proposed by Cheng [19] that takes into account micromechanical considerations. Cheng provided the relations between macromechanical and micromechanical parameters in the case of transverse isotropy. Abousleiman *et al.* [20], Abousleiman and Cui [21] and Cui *et al.* [22, 23] used this type of model in geomechanics and developed analytical solutions for wellbore and consolidation problems. Numerical applications of anisotropic poroelasticity can be found, among others, in Cui *et al.* [24], Kanj and Abousleiman [25] and Ekbote and Abousleiman [26].

In the following, we consider a porous medium that is composed of a deformable matrix and fully saturated by a liquid (subscript *lq*). The advection of the liquid is accounted for through Darcy's law. Isothermal conditions are assumed (due to climate control) such that the linear porous elastic model consists of one balance equation for liquid mass and linear momentum of the media.

1.1 Constitutive Equations for the Fully Saturated Medium

The non-linear poroelastic constitutive equations for the fully saturated media [28] are written incrementally. In the case of anisotropy, these constitutive equations have to be written in tensorial form as follows:

$$d\boldsymbol{\sigma} = \mathbb{C}\colon d\boldsymbol{\varepsilon} - \mathbf{B}dp_{lq} \tag{1}$$

$$\frac{dm_{lq}}{\rho_{lq}} = \mathbf{B}\colon d\boldsymbol{\varepsilon} + \left(\frac{1}{M_\phi} + \frac{\phi}{K_{lq}}\right)dp_{lq} \tag{2}$$

where $\boldsymbol{\sigma}$ and $\boldsymbol{\varepsilon}$ represent the second-order stress and strain tensors, respectively. p_{lq} refers to the liquid pressure. $\mathbb{C}$ is the fourth-order elasticity tensor, characterized by 2 Young's moduli (E_1, E_3), 2 Poisson coefficients (ν_{12}, ν_{13}) and a shear coefficient (G_{13}).

The components of the drained elastic stiffness tensor $\mathbb{C}$ of the porous medium can be found in Giot *et al.* [13].

$\mathbf{B}$ refers to the second-order tensor of the Biot coefficients, which can be written as follows:

$$\mathbf{B} = b_1(\mathbf{e_1}\otimes\mathbf{e_1} + \mathbf{e_2}\otimes\mathbf{e_2}) + b_3\mathbf{e_3}\otimes\mathbf{e_3} \tag{3}$$

M_ϕ is the solid Biot modulus and ϕ is the Lagrangian porosity. m_{lq}, ρ_{lq} and K_{lq} represent the liquid mass supply, the liquid density and the liquid compressibility, respectively. M_ϕ can be linked to the microscopic poroelastic properties of the matrix, the Biot coefficient and the porosity (Giot *et al.* [13] for details).

Concerning the microscopic poroelastic properties of the matrix, the components of the elastic tensor of the matrix $\mathbb{C}^s$ are given in Giot *et al.* [13]. The constitutive equations for the transverse isotropic poroelastic behaviour of the matrix can be written as follows:

$$d\boldsymbol{\sigma} = \mathbb{C}^s\colon d\boldsymbol{\varepsilon} - \mathbf{B}dp_{lq} \tag{4}$$

$$d\phi = \mathbf{B}\colon d\boldsymbol{\varepsilon} + \frac{dp_{lq}}{M_\phi} \tag{5}$$

Micro-macro relations can then be established for the Biot tensor and are detailed in Giot *et al.* [13]. It appears that the components of the Biot tensor are functions of 4 elastic moduli of the transverse isotropic elastic matrix tensor and on the corresponding 4 moduli of the transverse isotropic drained elastic tensor of the porous medium, which justifies that the same Biot tensor is considered for the fully saturated porous media and the matrix.

1.2 Conduction Equations

By applying Darcy's generalised law in a fully saturated medium and neglecting gravity, the velocity of liquid is ruled by:

$$\frac{\boldsymbol{M_{lq}}}{\rho_{lq}} = \boldsymbol{\lambda}^{\mathbf{lq}}.\left(-\nabla\boldsymbol{p_{lq}} + \rho_{lq}\boldsymbol{F^m}\right) \tag{6}$$

where $\boldsymbol{\lambda}^{\mathbf{lq}}$ designates Darcy's conductivity for liquid and is linked, for the fully saturated porous medium, to the intrinsic permeability $\mathbf{K}^{\mathbf{int}}$ through:

$$\boldsymbol{\lambda}^{\mathbf{lq}} = \mathbf{K}^{\mathbf{int}}(\phi)\frac{1}{\mu_{lq}} \tag{7a}$$

μ_{lq} represents the liquid dynamic viscosity. Darcy's conductivity for a liquid λ_{lq} is linked to liquid conductivity k_{lq}, which is homogeneous to a velocity ($\mathrm{m.s^{-1}}$), through:

$$\boldsymbol{\lambda_{lq}} = \frac{\mathbf{k_{lq}}}{\rho_{lq} g} \tag{7b}$$

Considering the transverse isotropy, the intrinsic permeability, and thus Darcy's conductivity, must be written as second-order tensors in the conduction equations as follows:

$$\mathbf{K^{int}} = K_1^{\text{int}}(\mathbf{e_1} \otimes \mathbf{e_1} + \mathbf{e_2} \otimes \mathbf{e_2}) + K_3^{\text{int}} \mathbf{e_3} \otimes \mathbf{e_3} \tag{8a}$$

$$\boldsymbol{\lambda^{lq}} = \lambda_1^{lq}(\mathbf{e_1} \otimes \mathbf{e_1} + \mathbf{e_2} \otimes \mathbf{e_2}) + \lambda_3^{lq} \mathbf{e_3} \otimes \mathbf{e_3} \tag{8b}$$

1.3 Momentum and Mass Conservation Equations

If we omit gravity, the linear momentum equation is written as follows:

$$\nabla.\sigma = 0 \tag{9}$$

The mass conservation equation for the liquid is expressed as follows:

$$\frac{\partial m_{lq}}{\partial t} = -\nabla.M_{lq} \tag{10}$$

1.4 Numerical Implementation and Model Parameters

The transverse isotropic poroelastic model was implemented in the finite element code Code_Aster (Edf), taking advantage of the isotropic poroelastic model available in Code_Aster [32-33]. The model was written for the general partially saturated case, and it also accounts for the couplings with thermal phenomena. Nevertheless, in this paper, we focus on the poromechanical couplings because the pulse test is assumed to be an isothermal process in which the temperature is fixed during the test. The parameters of the model, which were introduced in addition to the isotropic model, are:

- the elastic parameters of the skeleton: E_1^s, E_3^s, ν_{13}^s, ν_{12}^s and G_{13}^s, which can be assessed from measurements of the macromechanical parameters and micro-macro relations;
- the elastic parameters of the porous medium: E_1, E_3, ν_{13}, ν_{12} and G_{13};
- the hydromechanical coupling parameters of the Biot tensors: b_1 and b_3;
- the conduction parameters K_1^{int} and K_3^{int} for Darcy's law;
- the geometrical parameters (the 3 Euler angles, ϕ, θ, and ψ) which allow us to define the orientation of the isotropy planes (*Fig. 1*).

Moreover, as in the case of the axial pulse test, the model was simplified assuming micro-isotropy (Giot *et al.* [13]):

$$E_1^s = E_3^s = E^s; \nu_{12}^s = \nu_{13}^s = \nu^s \text{ and } G_{13}^s = G^s = \frac{E^s}{2(1+\nu^s)} \tag{11}$$

This assumption means that the solid constituent of the matrix is isotropic at the microscopic level. The macroscopic anisotropy comes from a structural origin and is a consequence of directional pore or fissure arrangement (Cheng [19]). This assumption is consistent with the actual knowledge of the microstructural elastic parameters of the studied rock type material. It reduces the number of elastic parameters to be assessed for the grain constituents. In the case of micro-isotropy assumption for the solid phase, the Biot tensor only depends on 4 elastic constants of the porous medium (E_1, E_3, ν_{13}, ν_{12}) and on the bulk modulus of the solid

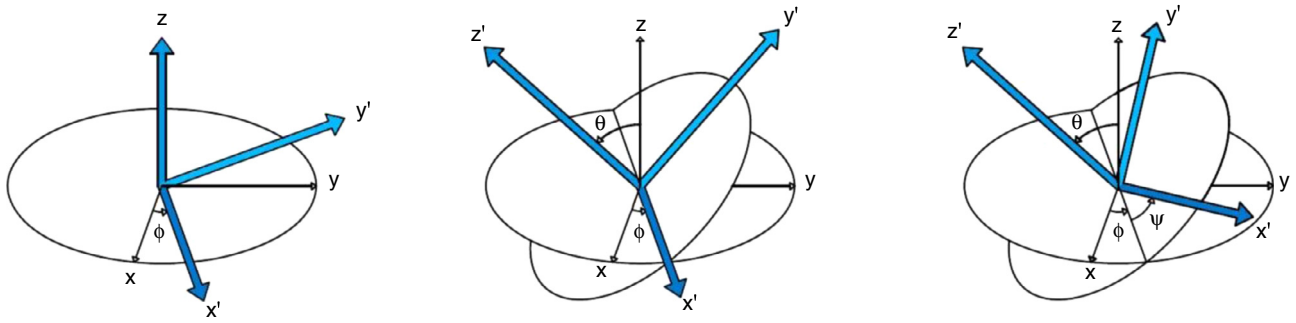

Figure 1

Euler angles convention.

phase k^s. The Biot tensor does not depend on the shear coefficients G_{13} and G^s.

2 RADIAL PULSE TEST: PRINCIPLE AND MODELING

2.1 Description of the Test

The experimental apparatus is presented in Figure 2. A hollow cylindrical rock sample, with an inner radius of 5 mm, an outer radius of 25 mm and a height of 50 mm, is placed in a load cell. Both the top and base of the sample are insulated to prevent water and air flow. The inner hole is connected to an upstream reservoir, while the outer boundary of the sample is connected to a downstream reservoir. The height of the inner chamber, which is connected to the upstream reservoir, is 30 mm and is less than the height of the sample. The diameter of the sample is less than the diameter of the cell. The remaining space between the sample and the body is 5 mm thick and is filled with silica glass balls of 1 and 2 mm diameters, which reproduces a porous network, allowing for the drainage of water, a homogeneous application of the confinement stress and a possible deformation of the sample. During the test, both the inner (upstream) and outer (downstream) pressures are measured using pressure sensors. Concerning the inner (upstream) pressure, it is measured using 2 different types of sensors. An internal sensor is placed in the cell, just under the draining wedge. This sensor consists of a little tablet that is 5 mm in diameter and 2 mm thick, with a resolution of 0.01 MPa. An external sensor, which also has a resolution of 0.01 MPa, is placed in the water circuit outside of the cell. Concerning the outer (downstream) pressure, it is not possible to place an internal sensor in the cell at the circumference of the sample (as for the upstream pressure); therefore, the pressure is only measured using an external pressure sensor placed in the water circuit. During the test, the temperature is maintained constant at 22°C thanks to a climate control. This climate control functions with successive cycles of emission of hot and cold air, lasting 5 minutes each. The external pressure sensors, for both the upstream and downstream chambers, are directly connected to those cycles of climate control; therefore, they exhibit pressure oscillations. The effects of the climate control are damped for the internal sensor placed in the cell, and as a consequence, the oscillations are softened.

The measurement system was calibrated based on a long time experiment (more than 15 years) on permeability measurements on very low permeability claystones, and particularly with the axial pulse test.

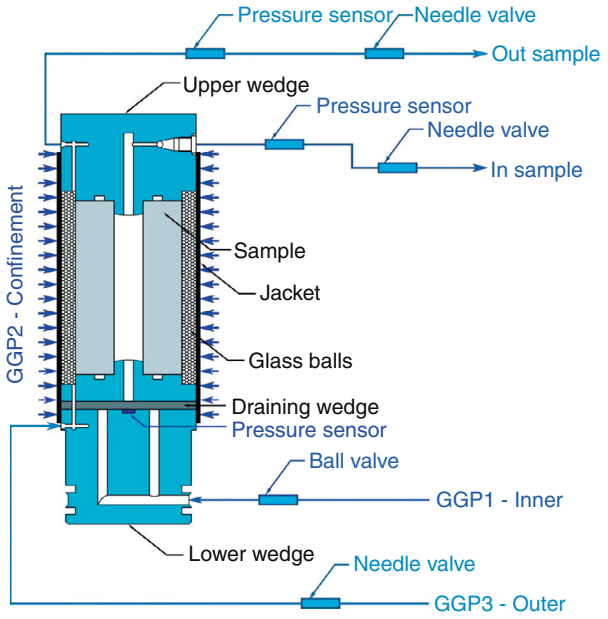

Figure 2

Experimental apparatus for the radial pulse test.

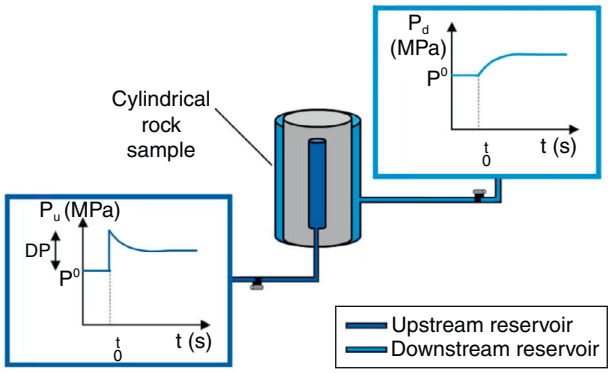

Figure 3

Principle of the radial pulse test.

Moreover, numerical modeling of the test was achieved considering fictitious isotropic samples for the design of the test.

The principle of the test is illustrated in Figure 3. The test is similar to the axial pulse test. After sample saturation and pore pressure homogenisation, the pressure is suddenly increased in the upstream reservoir (connected to the inner hole of the sample). The evolution of the pressures in the upstream (connected to the inner hole) and downstream (connected to the external

circumference of the sample) reservoirs are then measured. Because the length of the inner chamber is shorter than the length of the sample, the flow is bi-dimensional (both axial and radial); previous works have demonstrated that the flow is purely axial in the case of the axial pulse test. As a consequence, as will be shown *infra*, both axial and radial permeabilities are stimulated in the radial pulse test.

2.2 Initial and Boundary Conditions

In addition to the field and constitutive equations presented in Section 2, initial and boundary conditions for the radial pulse test must be expressed. The cylindrical sample of inner radius R_{in}, outer radius R_{ou}, and height L is submitted to a hydrostatic stress state. The sample is initially fully saturated, and both the liquid pressure and mean stress inside the sample are homogeneous:

$$p_{lq}(\mathbf{x}, t=0) = p_{lq}^0 \tag{12}$$

$$\sigma_m(\mathbf{x}, t=0) = \sigma_m^0 \tag{13}$$

In these equations, $\mathbf{x}$ denotes the position vector. The base Γ_0 and top Γ_L of the sample are insulated:

$$\mathrm{M_{lq}}.\mathrm{n} = 0 \quad \text{on } \Gamma_0 \text{ and } \Gamma_L \tag{14}$$

The liquid pressure is assumed to be homogeneous in both the upstream ($r = R_{in}$) and downstream ($r = R_{ou}$) reservoirs, where r represents the radial coordinate:

$$p_{lq}(\mathrm{z}, t) = p_{re}^u(t) \quad \text{on } \Gamma_{Rin} \tag{15a}$$

$$p_{lq}(\mathrm{z}, t) = p_{re}^d(t) \quad \text{on } \Gamma_{Rou} \tag{15b}$$

Γ_{Rin} is the circumference corresponding to the inner hole minus the first centimetres in the base and on the top of this hole. The height of the inner chamber for liquid injection is 30 mm, compared with the 50 mm height of the sample. The rest of the inner surface is insulated, like the top and base of the sample.

The liquid pressure is suddenly increased in the upstream reservoir:

$$p_{re}^u(0^+) = p_{lq}^0 + \Delta p \tag{16}$$

The conservation of liquid mass provides the 2 boundary conditions between the sample and the reservoirs:

$$\frac{\partial \xi^{\mathrm{u}}}{\partial t} = \int_{\Gamma_{\mathrm{Rin}}} -\lambda_{\mathrm{lq}} \nabla \mathrm{p_{lq}}(\mathrm{z}, \mathrm{t}).\mathrm{nda} \tag{17a}$$

$$\frac{\partial \xi^{\mathrm{d}}}{\partial t} = \int_{\Gamma_{\mathrm{Rou}}} -\lambda_{\mathrm{lq}} \nabla \mathrm{p_{lq}}(\mathrm{z}, \mathrm{t}).\mathrm{nda} \tag{17b}$$

$$\xi^u = \frac{M_{lq}^u}{\rho_{lq}} \quad \xi^d = \frac{M_{lq}^d}{\rho_{lq}} \tag{17c}$$

M_{lq}^u, M_{lq}^d, ξ^u and ξ^d represent the masses and volumes of liquid contained in the upstream and downstream reservoirs, respectively. Design tests on the experimental apparatus with a steel sample allowed for the assumption of a linear relationship between the volume of liquid content in the reservoirs and the liquid pressure. This linear relationship can be accepted in the tested range of pore pressures and for the increase of pressure considered in the tests. This relationship permits us to write the following equations:

$$\xi^u = \frac{p_{re}^u}{C_{re}^u} \quad \xi^d = \frac{p_{re}^d}{C_{re}^d} \tag{18}$$

The 2 coefficients $C_{re}^u$and C_{re}^d denote the stiffnesses of the reservoirs that can be bound to the reservoir storage coefficients S_{re}^u and S_{re}^d through:

$$C_{re}^u = \frac{\gamma_{lq}}{S_{re}^u} \quad C_{re}^d = \frac{\gamma_{lq}}{S_{re}^d} \tag{19}$$

γ_{lq} represents the volumetric weight of liquid. The boundary conditions between the reservoirs and the rock sample can then be expressed as:

$$\int_{R_{in}} -\lambda_{lq} \nabla \mathbf{p}_{\mathrm{lq}}(\mathbf{x}, t).\mathbf{n} da = \frac{1}{C_{re}^u} \frac{\partial p_{lq}(\mathbf{x}, t)}{\partial t} \quad p_{lq}(\mathbf{x}, t) p_{re}^u(t) \quad \text{on } \Gamma_{R_{in}} \tag{20a}$$

$$\int_{R_{ou}} -\lambda_{lq} \nabla \mathbf{p}_{\mathrm{lq}}(\mathbf{x}, t).\mathbf{n} da = \frac{1}{C_{re}^d} \frac{\partial p_{lq}(\mathbf{x}, t)}{\partial t} \quad p_{lq}(\mathbf{x}, t) p_{re}^d(t) \quad \text{on } \Gamma_{R_{ou}} \tag{20b}$$

The boundary conditions were implemented within the finite element code Code_Aster (Edf) through the adaptation of Fortran routines developed in the framework of the 3D numerical modeling of the axial pulse test (Giot *et al.* [13]). The integration was carried out with a Gaussian quadrature method, and an explicit time integration scheme was considered for implementing the boundary conditions (20):

$$p_{re}^u(t_{n+1}) = p_{re}^u(t_n) + C_{re}^u \Delta t \int_{R_{in}} -\lambda_{lq} \nabla \mathbf{p_{lq}}(\mathbf{z}, t_n).\mathbf{n} \mathrm{da} \tag{21a}$$

$$p_{re}^d(t_{n+1}) = p_{re}^d(t_n) + C_{re}^d \Delta t \int_{R_{ou}} -\lambda_{lq} \nabla \mathbf{p_{lq}}(\mathbf{z}, t_n).\mathbf{n} \mathrm{da} \tag{21b}$$

2.3 Geometry and Mesh

The geometry of the radial pulse allows us to focus on a 2D-axisymmetrical mesh. Thus, only half of the sample could be represented with a vertical symmetry axis. Nevertheless, the present work aims at investigating the effects of anisotropy. Except for the case of isotropy planes normal to the axis of the sample, the whole sample has to be considered and the geometrical model must be fully 3D. Figure 4 shows the geometry and mesh considered for the modeling. Several meshes, of different fineness or coarseness, were considered for the modeling. The mesh presented in Figure 4 is a simplified one. For the accuracy of the calculation, the mesh was refined on the inner and outer circumferences of the hollow cylinder. This refinement improves the calculation of the fluxes on these boundaries.

2.4 Main Results

Based on the results of the axial pulse test (Giot *et al.* [9, 13]), a sensitivity analysis was conducted on 2 types of anisotropic parameters, transfer parameters, more precisely intrinsic permeabilities K_1^{int} and K_3^{int}, and deformability parameters, specifically Young's moduli E_1 and E_3. Concerning the coupling parameters, Biot coefficients b_1 and b_3, they are linked to the Young's moduli through the specific storage coefficient, and thus we decided to focus on œdometric tests for the assessment of these parameters. Moreover, the previous works on the axial pulse test showed strong correlations between the Biot coefficients and the Young's moduli. Finally, the selected parameters control both the transient evolution (liquid diffusivity, D) and the final equilibrium (specific storage coefficient, S_s). In the isotropic case, the liquid diffusivity is defined as the ratio between the liquid conductivity k_{lq} and the specific storage coefficient:

$$D = \frac{k_{lq}}{S_S}$$

The reservoirs stiffnesses are intrinsic parameters of the experimental apparatus and are not impacted by anisotropy; thus, the stiffnesses were not considered to be of paramount importance when focusing on anisotropy, as they were for the axial pulse test.

In the following modeling, we considered both a transverse sample and a parallel sample to better understand the effects of the parameters on the results of the radial pulse test. The parameters with an index 1 represent the direction in the isotropy plane, whereas parameters with an index 3 represent the direction perpendicular to the isotropy plane. Each parameter will be either normal or axial, depending on the orientation of the sample.

2.4.1 Intrinsic Permeabilities

We first consider a transverse sample with the axis perpendicular to the isotropy planes. On such a sample, the axis of the sample coincides with the normal to the isotropy plane, denoted by $\mathbf{e}_3$. Figure 5 shows the curves

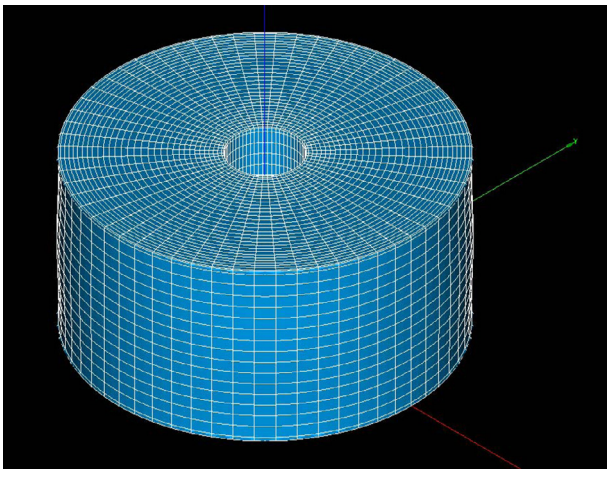

Figure 4

Example of a (simplified) 3D mesh used for numerical modeling of the radial pulse test.

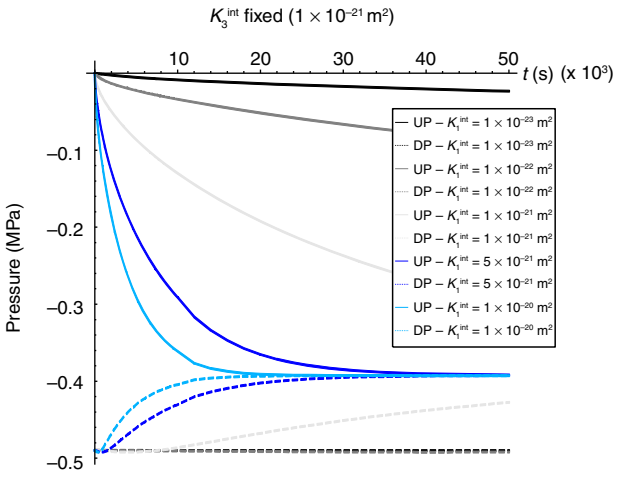

Figure 5

Evolution of reservoir pressure during the pulse test – influence of permeability K_1^{int} on the calculated pressure curves on the transverse sample (UP: Upstream pressure; DP: Downstream pressure).

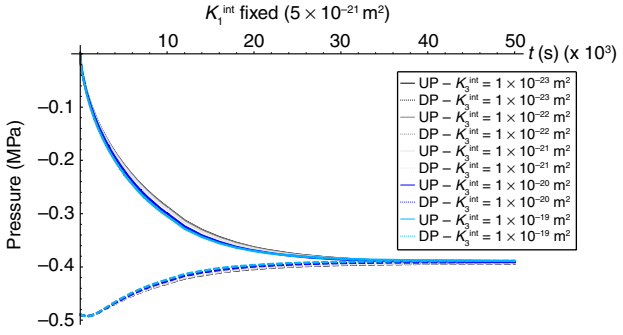

Figure 6

Evolution of reservoir pressure during the pulse test – influence of permeability K_3^{int} on the calculated pressure curves on the transverse sample (UP: Upstream pressure; DP: Downstream pressure).

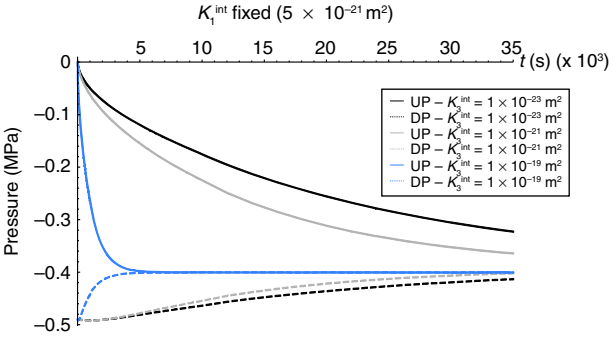

Figure 7

Evolution of reservoir pressure during the pulse test – influence of permeability K_3^{int} on the calculated pressure curves on the parallel sample (UP: Upstream pressure; DP: Downstream pressure).

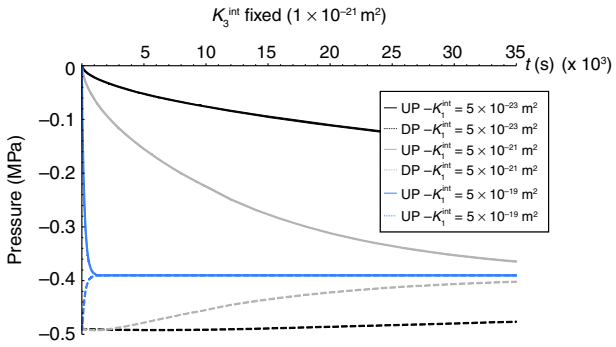

Figure 8

Evolution of reservoir pressure during the pulse test – influence of permeability K_1^{int} on the calculated pressure curves on the parallel sample (UP: Upstream pressure; DP: Downstream pressure).

of the calculated upstream and downstream pressures for such a transverse sample, with constant axial permeability K_3^{int} and varying radial permeability K_1^{int}. This means that in this sample, we vary the permeability in the direction perpendicular to the axis of the sample, thus in the direction of the isotropy plane. As expected, increasing K_1^{int} results in reaching equilibrium more quickly because intrinsic permeability controls the liquid diffusivity (transient evolution) and intrinsic permeability has no impact on the specific storage (final pressure equilibrium). Figure 6 presents the curves of the calculated upstream and downstream pressures for the same transverse sample but with constant radial permeability K_1^{int} and varying axial permeability K_3^{int}. The effect of changing K_3^{int} is less obvious than changing K_1^{int}. Once again increasing K_3^{int} results in reaching equilibrium more quickly, but this is less clear than for K_1^{int}. In fact, it appears that on such a transverse sample, the flow is mainly imposed in the direction of the isotropy plane that corresponds to the radial direction, and the hydraulic solicitation is mainly radial. As a consequence, the convergence of hydraulic solicitation and orientation of the isotropy planes favours a mainly radial flow and solicits the radial permeability K_1^{int}, while the permeability in the axial direction has little influence.

We can then consider the case of a parallel sample with the axis of the sample parallel to the isotropy plane. In such a case, the radial direction of the flow does not only coincide with the isotropy planes. Figure 7 presents the curves of the calculated upstream and downstream pressures for a parallel sample with constant axial permeability K_1^{int} and varying permeability K_3^{int}, with the direction $\mathbf{e}_3$ being a radial direction perpendicular to the axis of the sample. Once again, we can see that increasing K_3^{int} results in reaching equilibrium more quickly. Figure 8 presents the curves of the calculated upstream and downstream pressures for the same parallel sample, but with constant permeability K_3^{int} and varying permeability K_1^{int}. In this case, contrary to the transverse sample, the permeability K_1^{int} has a considerable influence. The influence is the same as for the other cases; increasing K_1^{int} results in reaching equilibrium more quickly. Therefore, in the case of the parallel sample, both intrinsic permeabilities influence the results of the radial pulse test. Indeed, in such a configuration, the boundary conditions that would favour a radial flow do not coincide with the isotropy planes, and thus boundary conditions (hydraulic solicitation) and geometrical configuration do not act jointly in only stimulating the direction of the isotropy planes.

Based on these results, we can see that for transverse samples, the permeability K_1^{int} primarily controls the pressure curves obtained during the radial pulse test, whereas K_3^{int} has little influence. On the contrary, for parallel samples, both K_1^{int} and K_3^{int} control the pressure evolution. As a consequence, to identify both intrinsic permeabilities K_1^{int} and K_3^{int}, it is more convenient to consider parallel samples than transverse samples. Generally, the intrinsic permeability controls the liquid diffusivity (transient evolution) but not the specific storage (final pressure equilibrium).

2.4.2 Young's Moduli

We first consider a transverse sample with the axis perpendicular to the isotropy planes. Figure 9 shows the effects of Young's modulus E_1 (the Young's modulus in the isotropy plane) on the upstream and downstream pressure curves obtained during the radial pulse test. One can see that E_1 slightly influences the specific storage coefficient (final equilibrium of the pressure) and has little impact on the liquid diffusivity (transient evolution). Concerning E_3, Figure 10 presents the upstream and downstream pressure curves obtained on a transverse sample for different values of E_3, with E_1 being fixed. This figure clearly demonstrates that E_3 has no influence on the pressure curves, neither on the liquid diffusivity nor on the specific storage. This response is similar to the axial pulse test. Indeed, Giot *et al.* [13] showed that for the axial pulse test on a transverse sample, the axial Young's modulus E_3 has no influence on the final equilibrium and a very slight influence on the liquid diffusivity, whereas E_1 influences both the liquid diffusivity and the specific storage coefficient.

Figures 11 and 12 present the upstream and downstream pressure curves for a parallel obtained during the pulse test for different values of E_3 (E_1 fixed) and E_1 (E_3 fixed). One can see that both Young's moduli influence the specific storage and have little influence on the liquid diffusivity. The influence of E_3 is a little more obvious than the influence of E_1. Thus, for the intrinsic permeability, the parallel sample appears better adapted than the transverse sample for assessing the Young's moduli anisotropy. Nevertheless, both Young's moduli act the same way, with a decrease of the Young's moduli resulting in a decrease of the final pressure, whichever the modulus considered. This could hinder the simultaneous identification of both moduli in the same test.

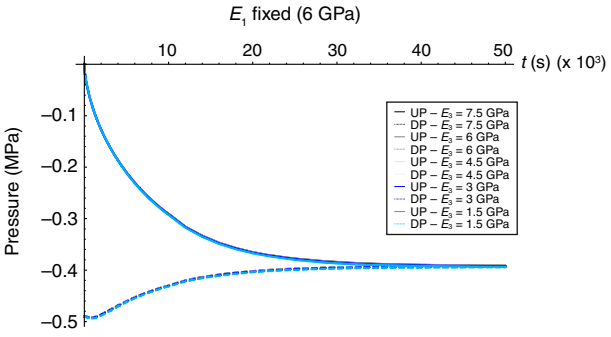

Figure 10

Evolution of reservoir pressure during the pulse test – influence of Young's modulus E_3 on the calculated pressure curves on the transverse sample (UP: Upstream pressure; DP: Downstream pressure).

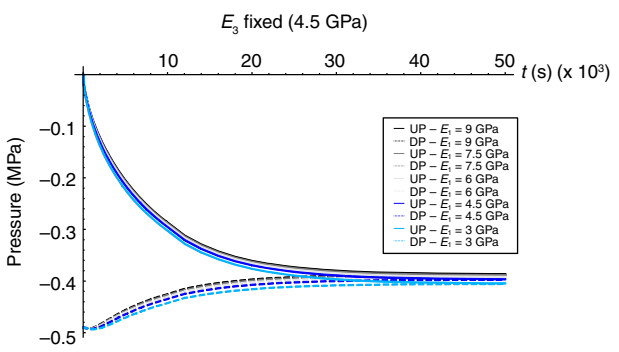

Figure 9

Evolution of reservoir pressure during the pulse test – influence of Young's modulus E_1 on the calculated pressure curves on the transverse sample (UP: Upstream pressure; DP: Downstream pressure).

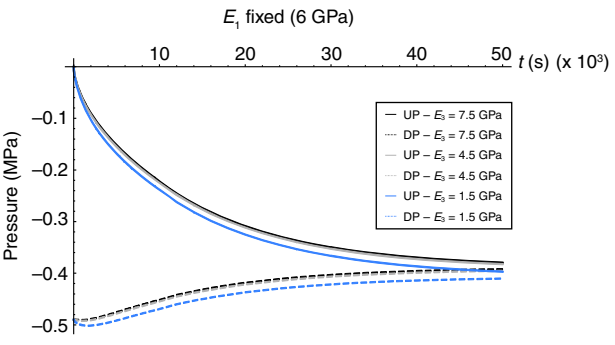

Figure 11

Evolution of reservoir pressure during the pulse test – influence of Young's modulus E_3 on the calculated pressure curves of the parallel sample (UP: Upstream pressure; DP: Downstream pressure).

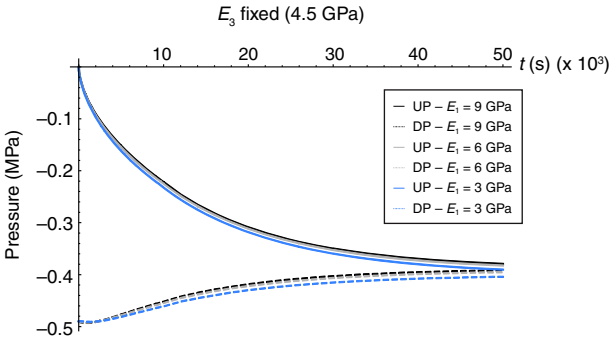

Figure 12

Evolution of reservoir pressure during the pulse test – Influence of Young's modulus E_1 on the calculated pressure curves of the parallel sample (UP: Upstream pressure; DP: Downstream pressure).

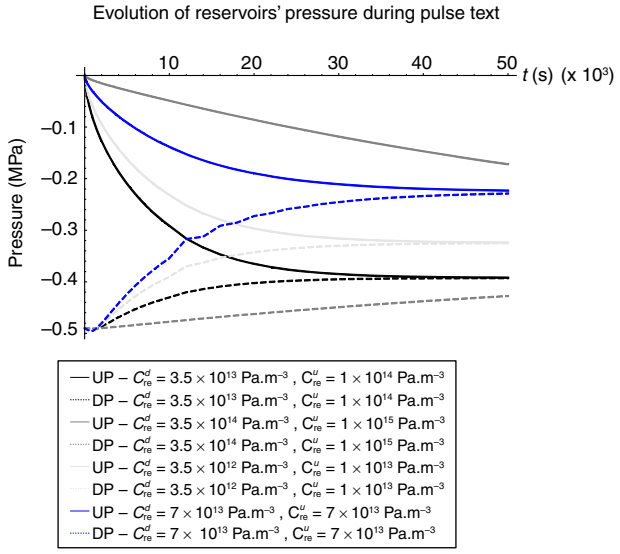

Figure 13

Evolution of reservoir pressure during the pulse test – influence of reservoir stiffnesses on the calculated pressure curves of the transverse sample (UP: Upstream pressure; DP: Downstream pressure).

In general, one can note that the tendency is the same for all of the modeling: the greater the Young's modulus, the greater the value of the pressure at final equilibrium.

2.4.3 Reservoir Stiffnesses

Figure 13 presents the upstream and downstream curves obtained during a radial pulse test on a transverse sample and for different values of the reservoir stiffnesses. The final equilibrium is achieved more quickly with an increase of the reservoir stiffness. This figure also shows that the reservoir stiffness influences both the kinetics of the test and the final equilibrium. In that way, the reservoir stiffnesses can influence the identification of both the liquid diffusivity and the specific storage. It is then required to have knowledge of the reservoir stiffness before the test or incorporate it in the set of parameter to identify. Nevertheless, the last solution is less efficient because the identification of the values of the stiffnesses could interfere in the identification of the other parameters.

3 INVERSE PROBLEM: INTERPRETATION OF LABORATORY PULSE TESTS

3.1 Inverse Method

Interpretation of the radial pulse test couples the numerical modeling (direct problem) with an inversion algorithm (inverse problem) to identify the uppermost liquid transport parameter and more specifically, the intrinsic permeability in the normal and parallel directions and possibly the poromechanical coupling parameters impacting the specific storage, such as the Biot coefficients and Young's moduli. This parameter identification problem is expressed as an optimisation problem aiming at minimising a cost-functional that quantifies the differences between experimentally measured and numerically calculated upstream and downstream pressures, which corresponds to an inverse problem that has been detailed in Giot *et al.* [9, 13]. The cost-functional is of the least-squares type and incorporates a term accounting for previous knowledge of the parameters, inferred, for example, from the interpretation of the classical axial pulse test performed on the same material:

$$\chi[\mathbf{c}] = \frac{1}{2}\sum_{i=1}^{Nmes} \omega_i(\gamma[\mathbf{c},\, t_i] - \gamma_{mes}[t_i])^2 + \frac{1}{2}\sum_{j=1}^{Npar} v_i\left(c_j - c_j^{prior}\right)^2 \tag{22a}$$

$$\gamma_{mes}[t_i] = p_{re}^{mes}[t_i] \tag{22b}$$

$$\gamma[\mathbf{c},\, t_i] = p_{re}^{u}[t_i] \quad \text{or} \quad \gamma[\mathbf{c},\, t_i] = p_{re}^{d}[t_i] \tag{22c}$$

In Equations (22), γ_{mes}, γ, $Nmes$, ω_i and v_j represent the measured and calculated pressure levels in the upstream and downstream reservoirs (that is, the pore pressures in the inner hole and at the circumference of the sample, respectively), the total number of measurements, and weighting coefficients on measurements and italic > a priori information, respectively. γ is a function of the parameters to be identified that make up the vector $\mathbf{c}$.

$\mathbf{c}^{\mathbf{prior}}$ consists of prior values of the parameters to be identified. p_{re}^{u} and p_{re}^{d} are calculated by finite element resolution of the previous system of Equations (1) to (21) expressing the direct problem of the radial pulse test.

Finally, the inverse problem of the pulse test may be formulated as follows:

$$\mathbf{c}^{\mathbf{identified}} = \arg\min[\chi[\mathbf{c}]]$$

The inverse method is of the probabilistic type. The minimisation algorithm is of the gradient type, the Levenberg-Marquardt algorithm to be more specific. This algorithm requires the assessment of the derivatives of the calculated pressures with respect to the parameters to be identified. This process corresponds to a sensitivity analysis that is conducted using a finite differences method.

From a numerical point of view, the second term of the cost-functional (22a), taking into account the prior knowledge of the parameters, smooths the cost-functional and decreases the probability of finding a local minimum, which is a common issue in inverse problems such as the one considered for the radial pulse test. The weighting coefficients w_i and u_j can be used to incorporate simple statistical information on both measurements and prior knowledge, and these terms stabilise the cost-functional. Moreover, these terms permit us to give relative importance to the prior knowledge in comparison with measurements, and consequently must be used with great care to avoid giving too much weight to this information. The weighting coefficients also allow us to render the cost-functional dimensionless, which is of paramount importance when several types of measurements of different orders are available (for example, pore pressures and deformations) as well as when several parameters are to be identified (also of different orders). This is the case of the radial pulse test because the gap between the intrinsic permeability and Young's moduli is of 30 orders of magnitude. The weighting coefficients on the measurements, ω_i, permit the consideration of the measurements' accuracy, and thus reduce the bias in parameter identification due to errors on pressure measurements. Errors on the measurements, which are on the order of the sensor's accuracy, should not result in a different solution to the inverse problem.

3.2 Correlations Between Parameters

Figures 14 and 15 provide the correlations between the sensitivities of both intrinsic permeabilities for a transverse and a parallel sample, respectively. The sensitivity of vector p_{re} of the reservoirs' pressures with respect to parameter c_i is generally given by:

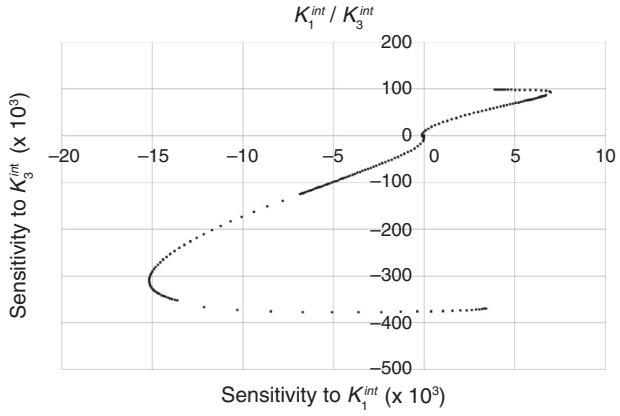

Figure 14

Correlations between the parameters' sensitivities for a transverse sample, example of intrinsic permeabilities.

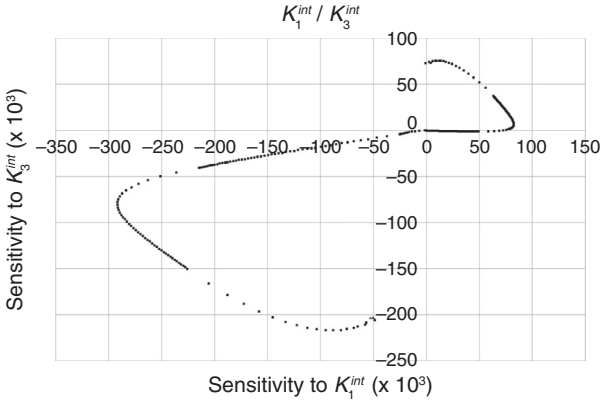

Figure 15

Correlations between parameters' sensitivities for a parallel sample, example of intrinsic permeabilities.

$$\delta_{c_i} p_{re} = \frac{\partial p_{re}}{\partial c_i} \tag{23}$$

For application to the radial pulse test, the sensitivity with respect to parameter c_i is assessed through a finite difference approximation:

$$\delta_{c_i} p_{re} = \frac{p_{re}[c_i + \Delta c_i] - p_{re}[c_i]}{\Delta c_i} \tag{24}$$

Although the sensitivities between all possible couples of parameters (intrinsic permeabilities and Young's moduli) for both transverse and parallel samples were studied, we confine ourselves to presenting the

correlations between the sensitivities of intrinsic permeabilities (because the others are similar and the analysis is still valid). The linear correlation coefficient $R(i, j)$ between the sensitivities with respect to parameters c_i and c_j is given by:

$$R(i,j) = \frac{cov(i,j)}{\sqrt{var(i)}\sqrt{var(j)}} \quad (25)$$

where $cov(i,j)$ denotes the covariance between parameters c_i and c_j, and $var(i)$ is the variance of parameter c_i.

$R(i, j)$ was calculated for all the couples of parameters and was significantly less than 1, confirming that no linear correlation could be identified between parameters. Thus, from these correlations, it appears that there is no clear linear relation between the parameters on which we decided to focus for the interpretation of the radial pulse test. Nevertheless, on each curve, one must distinguish 2 parts, one corresponding to the correlations concerning the upstream reservoir pressures, and the other concerning the downstream reservoir pressure. Due to the effects of climate control on the external pressure sensors, we decided to primarily focus on the upstream reservoir pressure for parameter identification. Then, it seems wise to confine the correlations to the upstream reservoir pressures. In such a case, the correlation coefficients are still low, always less than 0.7, indicating that no linear correlation can be identified between the parameters, except for the Young's moduli for a parallel sample (*Fig. 16*, $R^2 = 0.99$). Indeed, for such a sample, both moduli are solicited during the radial pulse test and, as shown in Figures 11 and 12, both parameters have the same influence on the pressure curves. This result confirms the previous observations and makes it difficult to identify the Young's moduli on a parallel sample. Nevertheless, the identification of these parameters is still interesting because we already have knowledge of these parameters and only want to identify as accurate values as possible. The main parameter being estimated through the pulse test is the intrinsic permeability, and the asset of the radial pulse test is the simultaneous identification of the intrinsic permeabilities in directions both parallel and normal to the isotropy planes. It is interesting to see that no clear correlations can be identified for these parameters, especially for the measurements of the pressures in the upstream reservoir on which we focused (for experimental reasons). More specifically, no correlation can be found between both permeabilities on both types of samples. As a consequence, there is no limitation on the simultaneous identification of both permeabilities, *i.e.*, the assessment of one permeability does not influence the assessment of the other permeability.

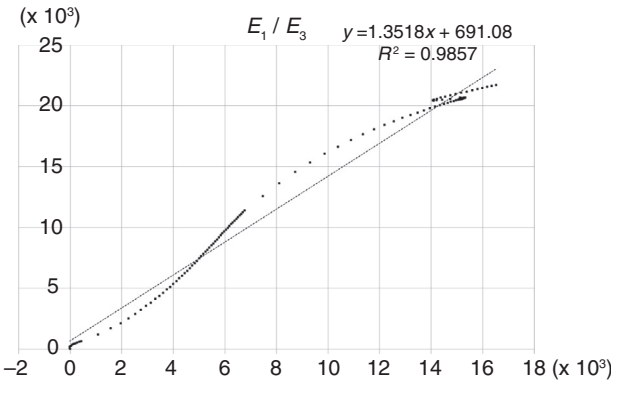

Figure 16

Correlations between parameters' sensitivities for a parallel sample, example of Young's moduli for upstream pressure.

3.3 Parameters to be Identified

The previous work on the classical axial pulse test showed that anisotropy does not concern the reservoirs' stiffnesses, which are intrinsic parameters of the experimental apparatus. Moreover, strong correlations were found between those stiffnesses and the rheological parameters (permeability, Young's modulus and Biot coefficient); the values of the reservoirs' stiffnesses influence the transient evolution and the final equilibrium, which are, respectively linked to the permeability and storage coefficient, the latter being a function of Young's modulus and Biot coefficient. As a consequence, we focused on the identification of rheological parameters and left the stiffnesses aside for the inverse problem. Additionally, strong correlations between the Young's modulus and Biot coefficient were observed in the isotropic case. Moreover, in the anisotropic case, it can be shown that the Biot coefficients can be expressed as functions of Young's moduli (Giot *et al.* [13]). Therefore, to limit the number of parameters to be identified, the identification was limited to intrinsic permeabilities, which influences the transient behaviour, and the Young's moduli, which influences the specific storage (the final equilibrium). When considering transverse isotropy for the classical axial pulse test (Giot *et al.* [13]) and based on a sensitivity analysis, the identification process focused on 4 parameters: the "axial" permeability, that is to say, K_1^{int} for the parallel samples and K_3^{int} for the transverse samples; and the "normal" Young's moduli, that is to say, E_1 for the transverse samples and E_3 for the axial samples. Thus, the identification focused on

2 parameters for each sample, which were the "axial" intrinsic permeability and the "normal" Young's modulus.

In comparison to the axial pulse test, the aim of the radial pulse test is to simultaneously identify both the axial and normal intrinsic permeabilities and Young's moduli on the same sample. The sensitivity analysis and the assessment of the correlations between these 4 parameters show that such identification is possible and that the only correlation that can be found is between both Young's moduli for a parallel sample (for upstream pressure). Nevertheless, the sensitivity analysis showed that only K_1^{int} could be identified for the transverse samples, whereas both K_1^{int} and K_3^{int} could be identified when considering parallel samples. The intrinsic permeabilities are the paramount parameters for the pulse test; therefore, we decided to focus on parallel samples for the identification of both intrinsic permeabilities. The price to pay is that the identification of both Young's moduli is more delicate for the parallel samples due to the strong correlation that exists between both parameters for such samples, more so because the identification favours the upstream pressure measurements (because of effects of climate control on downstream pressure) and the strong correlation concerns these upstream measurements. As a consequence, this correlation prevents the gradient-based inverse method being used for a wide range of values of the Young's moduli. In such a case, as for the inversion of the axial pulse test, the identification method presented previously must be coupled to a preliminary direct search method. The results of the direct search method and the previous knowledge on the Young's moduli are introduced in the gradient-based inverse method to define the *a priori* information as well as the initial values and tight boundaries on these parameters. Regarding the Young's moduli, the gradient-based inversion is then an optimisation or correction measure aiming at identifying the most accurate values in the range of values assessed by the direct search method.

Finally, the parameters to be identified can be noted as follows:

$$\mathbf{c}^{\mathbf{identified}} = \left\{K_1^{int\,opt}, K_3^{int\,opt}, E_1^{opt}, E_3^{opt}\right\}$$

3.4 Application

The inverse method combined with numerical modeling of the radial pulse test was applied to the interpretation of laboratory tests on 2 hollow cylindrical samples on Meuse/Haute-Marne claystones, a soft rock exhibiting transverse isotropy. Both samples were parallel samples to allow the identification of both permeabilities in the directions parallel and normal to isotropy planes. The physical data, dimensions and tests conditions are provided in Table 1.

Tables 2 and 3 give the values of the identified parameters in each case as well as the initial and *a priori* information values used to initiate the inverse analysis. Figures 17 and 18 present the experimental and fitted numerical curves obtained after the identification for both samples. One can observe the oscillations due to climate control in the experimental downstream pressure curves. The downstream pressure is measured using an external pressure sensor, while the upstream pressure is measured using an internal pressure sensor placed in the cell, which is less subjected to the climate control effects. As a consequence, the fitting is quite fair for the upstream pressure and better than for the downstream pressure. Indeed, we gave priority in the inversion method to the upstream pressure because its measurement is easier, more accurate and more reliable than the measurement of downstream pressure. This priority was achieved through the weighting parameters ω_i on measurements in the cost-functional (22a). For the upstream pressure, both the transient evolution and the final level are well reproduced numerically, indicating that both the intrinsic permeabilities and the Young's moduli were fairly identified, respectively.

For both samples, a meaningful set of parameters was identified. The values of permeabilities and Young's moduli obtained after inversion are consistent with the intrinsic permeability values, and tend to lie in the upper

TABLE 1
Physical data, dimensions and test conditions

Sample	44368-2	44368-3
Inner diameter (m)	0.0095	0.0095
Outer diameter (m)	0.04935	0.04969
Height (m)	0.05106	0.05005
Depth (m) NGF	−123.62	−123.62
Porosity	0.18	0.18
Orientation	Parallel to bedding	Parallel to bedding
Confinement (MPa)	4	4
Initial pore pressure (MPa)	1.00	1.02
Pore pressure increment (MPa)	0.41	0.40

range of values for the considered claystone. This result could be explained by the development of micro-cracks during drilling of the inner hole, which generates a damaged zone around this inner hole, increasing the permeability in that zone. For both samples, it appears that the anisotropy of transfer coefficients (permeabilities) is quite low, with a K_1^{int}/K_3^{int} ratio of 1.10 and 1.18 for samples 44368-2 and 44368-3, respectively. On the contrary, the mechanical anisotropy is much more marked, with a E_1/E_3 ratio of 2.14 for sample 44368-2 and a ratio of 1.28 for sample 44368-3. This result is similar to the one obtained for axial pulse tests (Giot *et al.* [13]). One can note that the anisotropy is less expressed for sample 44368-3 than for sample 44368-2 (*Tab. 4*).

TABLE 2
Results of the inversion on pulse test 44368-2

	Initial value	*A priori* value	Boundaries	Identified value
K_1^{int} (m^2)	8.0×10^{-20}	2×10^{-20}	1×10^{-23} / 1×10^{-18}	1.67×10^{-19}
K_3^{int} (m^2)	8.0×10^{-20}	2×10^{-20}	1×10^{-23} / 1×10^{-18}	1.51×10^{-19}
E_1 (Pa)	4.5×10^9	4.5×10^9	1×10^9 / 12×10^9	3.25×10^9
E_3 (Pa)	3.0×10^9	3×10^9	1×10^9 / 12×10^9	1.52×10^9
Nb iterations	11			

TABLE 3
Results of the inversion on pulse test 44368-3

	Initial value	*A priori* value	Boundaries	Identified value
K_1^{int} (m^2)	1.67×10^{-20}	2×10^{-20}	1×10^{-23} / 1×10^{-18}	1.44×10^{-19}
K_3^{int} (m^2)	1.51×10^{-20}	2×10^{-20}	1×10^{-23} / 1×10^{-18}	1.22×10^{-19}
E_1 (Pa)	3.25×10^9	4.5×10^9	1×10^9 / 12×10^9	6.77×10^9
E_3 (Pa)	1.52×10^9	3×10^9	1×10^9 / 12×10^9	5.27×10^9
Nb iterations	10			

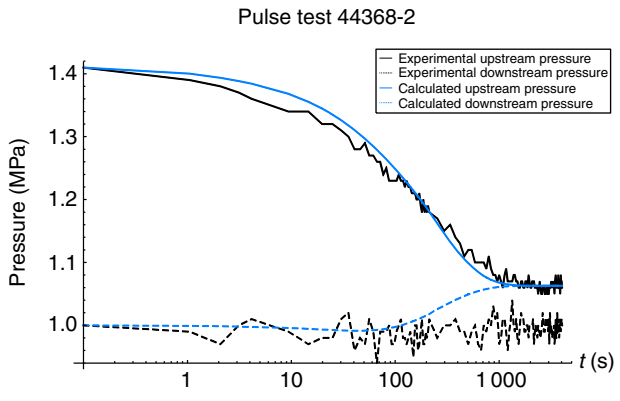

Figure 17

Pulse test 44368-2: comparison between experimental and fitted reservoir pressures.

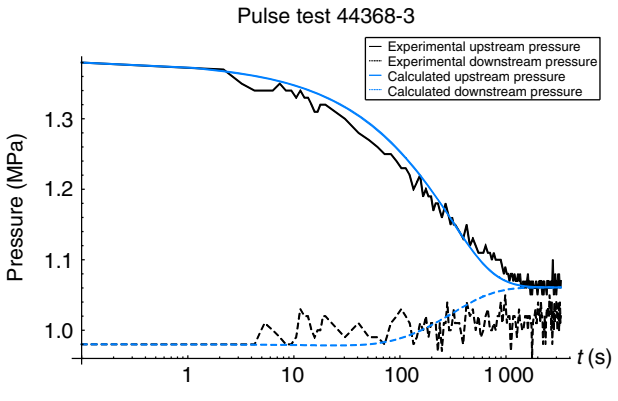

Figure 18

Pulse test 44368-3: comparison between experimental and fitted reservoir pressures.

TABLE 4
Comparison of the parameters inferred for both tests

Sample	44368-2	44368-3
Orientation	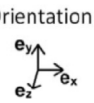	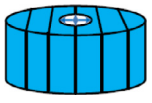
K_1^{int} (m^2)	1.67×10^{-19}	1.44×10^{-19}
K_3^{int} (m^2)	1.52×10^{-19}	1.22×10^{-19}
E_1 (GPa)	3.25	6.77
E_3 (GPa)	1.52	5.27

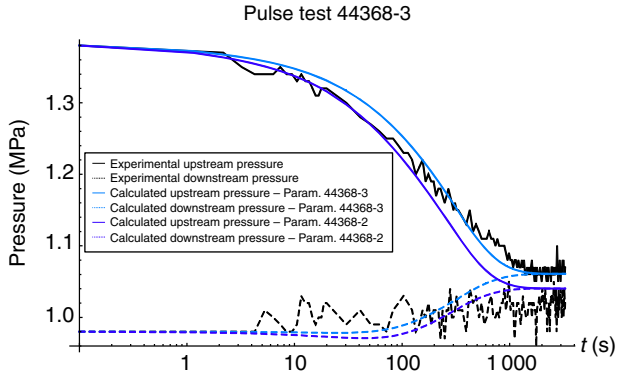

Figure 19

Pulse test 44368-3: comparison between experimental, fitted reservoir pressures and reservoir pressures calculated with the set of parameter identified on sample 44368-2.

The difference between the values identified for the intrinsic permeabilities and the Young's moduli between both samples may be explained by the heterogeneity of the rock mass, even if the samples are taken from the same borehole. This difference is not a consequence of the inversion method, as shown in Figure 19. This figure presents a comparison between the experimental curves for sample 44368-3, the calculated curves with the set of parameters identified on sample 44368-3 and the calculated curves with the set of parameters identified on sample 44368-2. This figure shows that the inverse procedure on sample 44368-3 gives a better fitting; the difference on the values of parameters identified is due to experimental data rather than to the identification process.

Let us note that for sample 44368-2, the inversion was conducted in 2 steps as follows: first, identification of both intrinsic permeabilities, with fixed values of the Young's moduli; then a second identification with the 4 parameters, considering for the permeabilities the values identified through the first identification. For sample 44368-3, we chose the parameter set identified on sample 44368-2 as the initial iterate because both samples were extracted from the same cell, and were thus geographically quite similar. In both cases, the value of the cost-functional was significantly reduced, by one order of magnitude for sample 44368-2, and half an order of magnitude for sample 44368-3 (for which the initial set was closer to the minimum because it integrated the results of the identification on sample 44368-2). The convergence was obtained on a condition on the gradient of the cost-functional, where the values of the parameters did not change significantly (less than 1% of the value) from one iteration to the next. To ensure the uniqueness of the solution, we tried different initial sets, but always in the same range of values, and verified that the same minimum was given by the identification process. This is mainly allowed by the first direct search step of the identification process, which always provides sets of parameters rather similar to the final set (corresponding to the minimum of the cost-functional (22a) used for the gradient based inversion algorithm).

Finally, let us add that a slight modification of the data (on the order of 10%) does not modify the values of the identified parameters, which means that the inversion method is robust. This is due to the consideration of the weighting parameters ω_i on the measurements in the cost-functional. Indeed, these terms smooth the cost-functional, taking into account the uncertainties or inaccuracies on the measurements. This process has always proven to be efficient on the axial pulse test and overcoring test, among others.

CONCLUSION

The interpretation of the axial pulse test on claystones, considering poromechanical couplings, underlined the anisotropy of this rock and the necessity to take anisotropy into account for the mechanical and transfer properties. Incorporating the transverse isotropy of the claystone in the poromechanical back-analysis of the test showed that 3D transverse isotropic modeling provides much more meaningful values of the identified parameters than the 2D isotropic modeling, particularly for the mechanical parameters. Nevertheless, these interpretations suffered from a lack a consistency on some results, which was attributed to the heterogeneity of the rock varying from one sample to the other. To overcome this problem, it was required to measure the 2 Young's moduli and 2 intrinsic permeabilities on the

same sample, and the radial pulse test was developed to achieve this aim.

The present paper addresses the radial pulse test, which consists in generating a sudden increase of pressure in the central hole of a hollow cylinder and measuring the evolution of pressure in the upstream (inner) reservoir and downstream (outer) reservoir. The interpretation is based on poromechanical numerical modeling, taking into account the transverse anisotropy's effects on the mechanical and transfer properties. The poromechanical modeling is coupled with an inverse method, as well as the poromechanical transverse isotropic constitutive law, with both being implemented in the finite element code Code_Aster (Edf).

The sensitive analysis performed on some parameters, including the intrinsic permeabilities and Young's moduli in directions both parallel and normal to the isotropy planes, showed that both intrinsic permeabilities could be identified during a single test only if parallel samples (cylindrical samples with the axis parallel to the isotropy planes) were considered. The identification of Young's moduli is more delicate due to a strong correlation between these 2 parameters and requires an adaptation of the inversion method. Indeed, the gradient-based inverse method must be coupled to a preliminary direct search method to reduce the range of variation in the values of the Young's moduli.

The identification method was used on laboratory tests on Meuse/Haute-Marne argillites, on parallel cylindrical samples with the axis parallel to the isotropy planes. The results are quite fair and encouraging, showing a clearer anisotropy on the mechanical parameters than on the transfer parameters.

In future works, the radial pulse test could be coupled to the classical axial pulse test on samples of the same origin, to characterize the effects of damage on rock permeability. Indeed, the configuration of the radial pulse test, *i.e.*, hollow cylinder, is close to the configuration of gallery excavation and can thus generate some type of excavation damaged zone at small scales. Comparing the values of the permeabilities identified on both pulse tests could allow identification of the effects of this damaged zone on permeability. This methodology could be used on isotropic samples, at first.

The next step of the present work is to identify some other poromechanical parameters to obtain a complete set of parameters for the claystone. To achieve this aim, other types of tests have to be considered and back-analysed using the inverse method presented in this paper, coupled with numerical modeling and accounting for the poromechanical transverse isotropic model. Drying tests allow identification of transfer parameters in partially saturated conditions (relative permeability and sorption isotherm, to be more specific), while the œdometric test allows the identification of Biot coefficients.

ACKNOWLEDGMENTS

This work was supported by ANDRA, Scientific Division, 1/7 rue Jean Monnet, 92290 Châtenay-Malabry, France. The author expresses sincere gratitude to the organization.

REFERENCES

1 Brace W.F., Walsh J.B., Frangos W.T. (1968) Permeability of granite under high pressure, *J. Geophys. Res.* **73**, 2, 2225-2236.

2 Hsieh P.A., Tracy J.V., Neuzil C.E., Bredehoeft J.D., Silliman S.E. (1981) A transient laboratory method for determining the hydraulic properties of tight rocks. I. Theory, *Int. J. Rock Mech. Min. Sci. Geomech. Abstr.* **18**, 245-252.

3 Neuzil C.E., Cooley C., Silliman S.E., Bredehoeft J.D., Hsieh P.A. (1981) A transient laboratory method for determining the hydraulic properties of tight rocks. II. Application, *Int. J. Roch Mech. Min. Sci. Geomech. Abstr.* **18**, 253-258.

4 Homand F., Giraud A., Escoffier S., Koriche A., Hoxha D. (2004) Permeability determination of a deep argillite in saturated and partially saturated conditions, *Int. J. Heat Mass Trans.* **47**, 3517-3531.

5 Selvadurai A.P., Letendre A., Hekimi B. (2001) Axial flow hydraulic pulse testing of an argillaceous limestone, *Environ. Earth Sci.* **64**, 2047-2058.

6 Wang H.F. (2003) *Theory of linear poroelasticity*, Princeton University Press, Princeton and Oxford.

7 Adachi J.I., Detournay E. (1997) A poroelastic solution of the oscillating pore pressure method to measure permeabilities of tight rocks, *Int. J. Rock Mech. Min. Sci. Geomech. Abstr.* **34**, 3-4, paper 062.

8 Walder J., Nur J. (1986) Permeability measurement by the pulse decay method: effect of poroelastic phenomena and non linear pore pressure diffusion, *Int. J. Rock Mech. Min. Sci. Geomech. Abstr.* **23**, 3, 225-232.

9 Giot R., Giraud A., Auvray C., Homand F., Guillon T. (2011) Fully coupled prormechanical back analysis of the pulse test by inverse method, *Int. J. Numer. Anal. Methods Geomech.* **35**, 3, 329-359.

10 Zhang C., Rothfuchs T. (2004) Experimental study of the hydro-mechanical behavior of the Callovo-Oxfordian argillite, *Appl. Clay Sci.* **26**, 325-336.

11 Cariou S., Duan Z., Davy C., Skoczylas F., Dormieux L. (2012) Poromechanics of partially saturated Cox argillite, *Appl. Clay Sci.* **56**, 36-47.

12 Marschall P., Horseman S., Gimmi T. (2005) Characterisation of Gas Transport Properties of the Opalinus Clay, a Potential Host Rock Formation for Radioactive Waste Disposal, *Oil Gas Sci. – Technol. Rev. IFP* **60**, 1, 121-139.

13 Giot R., Giraud A., Guillon T., Auvray C. (2012) Three-dimensional poromechanical back analysis of the pulse test accounting for transverse isotropy, *Acta Geotechnica* **7**, 151-165.

14 Giot R., Giraud A., Homand F. (2005) Three Dimensional modelling of stress relaxation tests with finite element in anisotropic clayey medium: direct problem and back analysis, *Geotech. Geol. Eng.* **24**, 919-947.

15 Alarcon-Ruiz L., Brocato M., Dal Pont S., Feraille A. (2010) Size Effect in Concrete Intrinsic Permeability Measurements, *Transport Porous Med.* **85**, 541-564.

16 Dal Pont S., Schrefler B.A., Ehrlacher A. (2005) Intrinsic Permeability Evolution in High Temperature Concrete: An Experimental and Numerical Analysis, *Transport Porous Med.* **60**, 43-74.

17 Davy C., Skoczylas F., Barnichon J.-D., Lebon P. (2007) Permeability of macro-cracked argillite under confinement: Gas and water testing, *Phys. Chem. Earth Parts A/B/C* **32**, 667-680.

18 Noiret A., Giot R., Bemer E., Giraud A., Homand F. (2011) Hydromechanical behavior of Tournemire argillites: measurement of the poroelastic parameters and estimation of the intrinsic permeability by œdometric tests, *Int. J. Numer. Anal. Methods Geomech.* **35**, 4, 496-518.

19 Cheng A.H.-D. (1997) Material Coefficient of Anisotropic Poroelasticity, *Int. J. Rock Mech. Min. Sci. Geomech. Abstr.* **34**, 2, 199-205.

20 Abousleiman Y., Cheng A.H.-D., Cui L., Detournay E., Roegiers J.-C. (1996) Mandel's problem revisited, *Geotechnique* **46**, 2, 187-195.

21 Abousleiman Y., Cui L. (1998) Poroelastic solutions in transversely isotropic media for wellbore and cylinder, *Int. J. Solids Structures* **35**, 34-35, 4905-4929.

22 Cui L., Abousleiman Y., Cheng A.H.-D., Roegiers J.-C. (1996) Anisotropy effect on one-dimensional consolidation, *ASCE, EM 11th conference*, FT Lauderdale, FL, May 19-22, pp. 471-474.

23 Cui L., Abousleiman Y., Roegiers J.-C. (1998) Solutions for hollow cyclinders in transversely isotropic porous materials, *Int. J. Rock Mech. Min. Sci.* **35**, 4-5, 635-636.

24 Cui L., Cheng A.H.D., Kaliakin V.N., Abousleiman Y., Roegiers J.-C. (1996) Finite element analysis of anisotropic poroelasticity: A generalized Mandel's problem and an inclined borehole problem, *Int. J. Numer. Anal. Methods Geomech.* **20**, 6, 381-401.

25 Kanj M., Abousleiman Y. (2005) Porothermoelastic analyses of anisotropic hollow cylinders with applications, *Int. J. Numer. Anal. Methods Geomech.* **29**, 2, 103-126.

26 Ekbote S., Abousleiman Y. (2006) Porochemoelastic solution for an inclined borehole in a transversely isotropic formation, *J. Eng. Mech.* **137**, 7, 754-763.

27 Lewis R.W., Schrefler B.A., Simoni L. (1991) Coupling *versus* uncoupling in soil consolidation, *Int. J. Numer. Anal. Methods Geomech.* **15**, 533-548.

28 Coussy O. (2004) *Poromechanics*, John Wiley and Sons, Paris, ISBN 0-470-84920-7.

29 Detournay E., Cheng A.H.-D. (1993) Fundamentals of poroelasticity, in *Comprehensive Rock Engineering: Principles, Practice and Projects, Vol. II, Analysis and Design Method*, Chapter 5, Fairhurst C. (ed.), Pergamon Press, Oxford, pp. 113-171.

30 Schrefler B.A., Gawin D. (1996) The effective stress principle: incremental or finite form? *Int. J. Numer. Anal. Methods Geomech.* **20**, 785-814.

31 Cheng A.H.D. (2008) Abousleiman Y. Intrisic poroelasticity constants and a semilinear model, *Int. J. Numer. Anal. Methods Geomech.* **32**, 7, 803-831.

32 Chavant C. (2001) Modélisations THHM, généralités et algorithmes, *Official Documentation of Code_Aster*, R7.01.10a, www.code-aster.org.

33 Chavant C., Granet S. (2005) Modèles de comportement THHM, *Official Documentation of Code_Aster*, R7.01.11b, www.code-aster.org.

Manuscript accepted in April 2013
Published online in November 2013